Contrasting impurity-induced magnetism and dynamics in $2H$-$MoTe_2$

Jonas A. Krieger,[1,*,†] Igor P. Rusinov,[2] Sourabh Barua,[3,‡] Aris Chatzichristos,[4,5] Jared Croese,[6] Derek Fujimoto,[4,5,§] Stefan Holenstein,[1,7] Victoria L. Karner,[5,8] Ryan M. L. McFadden,[5,8,§] John O. Ticknor,[5,8] W. Andrew MacFarlane,[5,8,9] Robert F. Kiefl,[4,5,9] Geetha Balakrishnan,[3] Evgueni V. Chulkov,[10,11,12] Stuart S. P. Parkin,[13] and Zaher Salman[1,‖]

[1]*PSI Center for Neutron and Muon Sciences, 5232 Villigen PSI, Switzerland*
[2]*Lebedev Physical Institute of the Russian Academy of Sciences, 119991 Moscow, Russia*
[3]*Department of Physics, University of Warwick, Coventry CV4 7AL, United Kingdom*
[4]*Department of Physics and Astronomy, University of British Columbia, Vancouver, British Columbia V6T 1Z1, Canada*
[5]*Stewart Blusson Quantum Matter Institute, University of British Columbia, Vancouver, British Columbia V6T 1Z4, Canada*
[6]*CERN, Esplanade des Particules 1, 1211 Geneva, Switzerland*
[7]*Physik-Institut der Universität Zürich, Winterthurerstrasse, 8057 Zürich, Switzerland*
[8]*Department of Chemistry, University of British Columbia, Vancouver, British Columbia V6T 1Z1, Canada*
[9]*TRIUMF, Vancouver, British Columbia V6T 2A3, Canada*
[10]*Departamento de Polímeros y Materiales Avanzados: Física, Química y Tecnología, Facultad de Ciencias Químicas, Aptdo. 1072, 20018 San Sebastián, Spain*
[11]*Institute of Strength Physics and Materials Science, Siberian Branch, Russian Academy of Sciences, 634055 Tomsk, Russia*
[12]*Laboratory of Electronic and Spin Structure of Nanosystems, Saint Petersburg State University, 198504 Saint Petersburg, Russia*
[13]*Max Planck Institut für Mikrostrukturphysik, Weinberg 2, 06120 Halle, Germany*

(Received 27 January 2026; accepted 22 May 2026; published 18 June 2026)

We investigate the behavior of interstitial $^8Li^+$ implanted near the surface of $2H$-$MoTe_2$ using β-detected nuclear magnetic resonance. We find that, unlike the muon, $^8Li^+$ does not show any signature of induced magnetism. This result is consistent with density functional theory, which identifies the Li stopping site at the 2a Wyckoff position in the van der Waals gap and confirms the absence of detectable Li-induced electronic spin polarization. Both the spin-lattice relaxation and the resonance line shape show evidence of pronounced spin dynamics above ∼200 K, reminiscent of local stochastic $^8Li^+$ motion within a cage. The resonance line shape consists of quadrupolar satellites on top of a broad central peak. To better understand the interaction of $^8Li^+$ with the host material, we employ a frequency-comb measurement by simultaneously exciting four frequencies corresponding to the first-order quadrupolar satellite transitions, $\nu_0 \pm 3\nu_{comb}$ and $\nu_0 \pm \nu_{comb}$, around the Larmor frequency ν_0 as a function of ν_{comb}. This offers an enhanced sensitivity to the quadrupolar split portion of the line. Using this method, we find a small decrease in the quadrupolar frequency with increasing temperature, showing the typical behavior associated with thermally excited phonons and the absence of any magnetic response, in contrast to what was observed for other defects in $2H$-$MoTe_2$.

DOI: 10.1103/49q2-5vl8

I. INTRODUCTION

Transition metal dichalcogenides (TMDs) are a family of layered van der Waals (vdW) materials consisting of stacks of MX_2 trilayers, where the transition metal M is surrounded by six chalcogenide atoms X, usually either with a trigonal prismatic (H) or with a distorted octahedral (T) coordination. Despite this similarity in atomic structure, these materials exhibit a plethora of different physical phenomena, ranging from metallic, semiconducting, Weyl-semimetallic, and superconducting to ferromagnetic, antiferromagnetic, and charge-density-wave behavior [1]. For this reason, they offer a considerable potential for vdW heterostructure engineering [2,3]. Semiconducting TMDs are of particular interest for integration into electronic and optical applications, for example, polymorphic $MoTe_2$, which in the hexagonal $2H$-phase has an indirect ∼1 eV band gap [4,5]. Interestingly, in the monolayer the band gap becomes direct, which has been exploited to build transistors and photodetector devices [6–8]. Furthermore, $2H$-$MoTe_2$ was recently predicted to be an obstructed atomic insulator, having Wannier charge centers located away from atomic

*Contact author: jonas.krieger@psi.ch
†Formerly at Max Planck Institut für Mikrostrukturphysik, Weinberg 2, 06120 Halle, Germany.
‡Present address: Department of Physics, Central University of Punjab, Bathinda 151401, India.
§Present address: TRIUMF, Vancouver, British Columbia V6T 2A3, Canada.
‖Contact author: zaher.salman@psi.ch

Published by the American Physical Society under the terms of the Creative Commons Attribution 4.0 International license. Further distribution of this work must maintain attribution to the author(s) and the published article's title, journal citation, and DOI.

positions [9]. As a result, it is expected to host obstructed surface states on nonbasal surfaces and line defects, associated with a high catalytic activity useful for hydrogen evolution reaction [9].

Semiconducting TMDs are particularly susceptible to impurity-induced magnetism arising from defects, interstitials, or adsorbates. In $2H$-$MoTe_2$, magnetic moments have been predicted at antisite defects [10], via hydrogen or transition metal doping of the monolayer [11,12], and most notably in association with hydrogenlike muonium impurities in the vdW gap [13]. While defects are also known to strongly modify optical, electronic, and catalytic properties [14–16], their magnetic impact remains subtle and probe dependent. In particular, muon spin relaxation (μSR) measurements consistently revealed clear signatures of magnetism. Originally attributed to intrinsic magnetic order [17], these results were subsequently reproduced in a crystal in which conventional ^{125}Te-nuclear magnetic resonance (NMR) found no intrinsic magnetic order, and were instead shown to be consistent with a magnetic muonium state—a bound state of a muon and an electron whose electronic spin is magnetically polarized along the c axis [13]. These results indicate that the observed magnetism is impurity induced rather than a bulk property of $2H$-$MoTe_2$.

Here, we present beta-detected nuclear magnetic resonance (β-NMR) data on spin-polarized $^8Li^+$ implanted into a $2H$-$MoTe_2$ single crystal. As a charged impurity likely occupying the vdW gap, $^8Li^+$ provides a direct comparison to the hydrogenlike muonium state detected by μSR. Despite occupying a similar crystallographic site, we observe no evidence of either intrinsic or impurity-induced magnetism. Instead, the spin-lattice relaxation and resonance line shape reveal the onset of pronounced local dynamics above ∼200 K. Using a frequency-comb detection scheme, we accurately determine the quadrupolar splitting even in the presence of an overlapping broad component. These results demonstrate that the magnetic behavior in $2H$-$MoTe_2$ and other semiconducting TMDs depends sensitively on the electronic character and charge state of the impurity, as well as its specific interaction with the host material.

II. EXPERIMENT

High-quality single crystals of $2H$-$MoTe_2$ were grown by chemical vapor transport, using $TeCl_4$ as a transport agent [13]. The crystal studied here was taken from the same batch as those studied in Ref. [13]. It was glued onto a sapphire substrate using silver paint and then mounted on a cold-finger cryostat. The surface of the crystal was initially cleaved but was kept in air for an extended period of time afterward. The β-NMR measurements were performed on the β-nuclear quadrupole resonance (β-NQR) [18] and β-NMR [19] spectrometers at the isotope separator and accelerator (ISAC) facility in TRIUMF, Vancouver, Canada [20–23]. Spin-polarized $^8Li^+$ (spin $I = 2$ and quadrupole moment $Q \sim 32$ mb with about 70% polarization [24]) was implanted with an energy of 22.5 keV along the c axis of the crystal. The corresponding ion-implantation stopping profile was simulated with the `TRIM.SP` [25] software (using mass density of 7.78 g/cm^3) and is shown in Fig. 1(a). We find that the average implantation depth of $^8Li^+$ is ∼110 nm. Note that the size of the crystal (∼25 mm^2) was large compared to the beam spot diameter (∼2 mm); thus, we expect no significant background signal from ions missing the sample. The spin-lattice relaxation rate (SLR) was measured in an in-plane magnetic field, $B \perp c$, and the line shape and frequency-comb measurements were performed in the presence of an out-of-plane field, $B \parallel c$. In both cases, the fields were applied parallel to the initial $^8Li^+$ nuclear spin direction. ^{8}Li is unstable, with a lifetime of $\tau_{^8\mathrm{Li}} = 1.2$ s and has an anisotropic β decay, with the preferential emission direction of the decay electron being opposite to the direction of the ^{8}Li nuclear spin [18,19]. This allows the measurement of the average spin direction of an ^{8}Li ensemble via the detection of the anisotropic decay electrons.

The ^{8}Li SLR was measured by implanting a 4 s pulse of $^8Li^+$ beam while monitoring the asymmetry in the emitted electrons during and after the beam pulse. The measured β asymmetry is proportional to the time evolution of the average nuclear spin polarization and therefore reflects the SLR rate of ^{8}Li.

The ^{8}Li resonance lines were measured by implanting ^{8}Li continuously and monitoring the decay asymmetry while sweeping a continuous-wave (CW) radio-frequency (RF) magnetic field through the resonance [19]. A quadrupole split resonance due to an electric field gradient (EFG) at the ^{8}Li stopping site appears in the spectra as a set of four small satellite lines in the vicinity of the Larmor frequency, ν_L. This splitting was measured by using a frequency comb instead of a single frequency [26,27]. This dramatically enhances the signal corresponding to the quadrupole satellites because the CW comb excites all four quadrupolar transitions simultaneously: $\nu_0 \pm \nu_\mathrm{comb}$ and $\nu_0 \pm 3\nu_\mathrm{comb}$, where ν_0 is the predetermined center of the line and ν_comb is the swept frequency parameter. A depolarization of the ^{8}Li spin ensemble due to the first-order quadrupolar transitions will therefore occur at the frequencies $\nu_\mathrm{comb} = \nu_q/3$, $\nu_\mathrm{comb} = \nu_q$, and $\nu_\mathrm{comb} = 3\nu_q$, where the quadrupolar frequency $h\nu_q = eQV_{zz}/8$ arises from the nuclear electric quadrupole moment eQ and the EFG at the ^{8}Li site, of which V_{zz} is the largest principal component. Note that on resonance (i.e., at $\nu_\mathrm{comb} = \nu_q$ and $\nu_0 = \nu_\mathrm{L}$), the depolarization of the ^{8}Li ensemble will be further enhanced, since multiple quadrupolar transitions can be excited simultaneously [28,29]. The center frequency ν_0 is chosen based on a preceding calibration measurement of the Larmor frequency. Therefore, it will only be accurate up to an error $\delta\nu_0$. As a consequence, the quadrupolar transitions will split and appear to be at $\nu_\mathrm{comb} = \nu_q/3 \pm \delta\nu_0/3$, $\nu_\mathrm{comb} = \nu_q \pm \delta\nu_0/3, \pm\delta\nu_0$, and $\nu_\mathrm{comb} = 3\nu_q \pm \delta\nu_0$. When the quadrupolar interaction is much smaller than the Zeeman energy in the applied field, this splitting is symmetric around the nominal transition frequency. Hence, as long as $\delta\nu_0$ is smaller than the width of the quadrupolar satellites, this splitting will not be visible and the effect of $\delta\nu_0$ can be neglected without degrading the accuracy of the determined ν_q. In these experiments, except for the measurement at room temperature, we are in this limit. It is important to point out here that $\delta\nu_0$ will affect in a nontrivial way the width and height of the peaks measured with the frequency comb, making this approach less suited

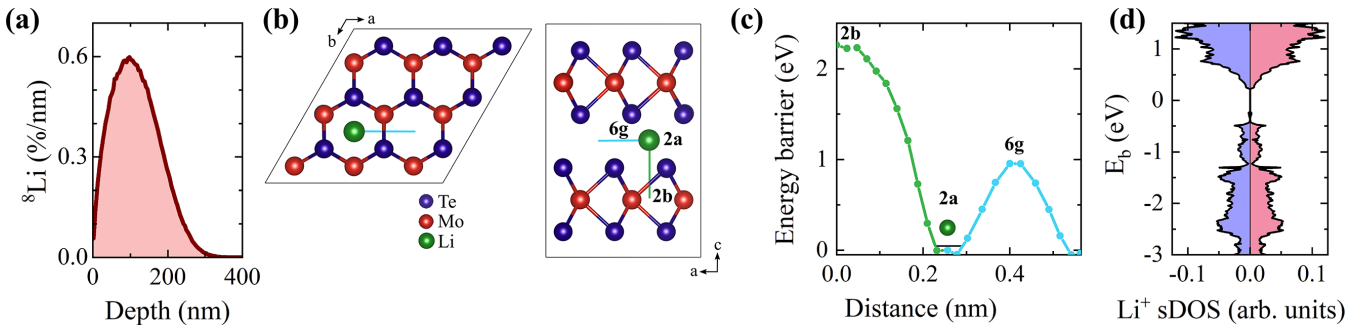

FIG. 1. (a) Simulated stopping profile of 22.5 keV $^8Li^+$ ions in $2H$-$MoTe_2$. (b) Calculated $^8Li^+$ stopping site in the van der Waals gap and representative diffusion paths between symmetry-equivalent sites. (c) Corresponding diffusion energy barriers obtained from density functional theory (DFT) nudged elastic band calculations. The high-symmetry sites along the $^8Li^+$ diffusion path are labeled by their Wyckoff positions in space group 194. (d) Spin-resolved density of states from DFT calculations for $2H$-$MoTe_2$ with an interstitial $^8Li^+$ impurity at the 2a site. The absence of a difference between spin-up and spin-down components indicates that the $^8Li^+$ impurity does not induce magnetic polarization. An induced magnetic moment would manifest as a clear spin asymmetry between the two spin channels.

for an accurate determination of the ^{8}Li's initial state population. All measurements (SLR, resonance, and frequency-comb measurements) have been performed while switching the initial polarization direction and, where applicable, the RF sweep directions. The resulting asymmetries were subtracted from each other to minimize systematic errors. The data were analyzed with the `musrfit` [30] software.

III. DFT CALCULATIONS

The ^{8}Li site and diffusion barriers were calculated with Density Functional Theory, consistent with the calculations used to determine the muon site in Ref. [13]. Lithium was introduced in a relaxed $3 \times 3 \times 1$ supercell of $2H$-$MoTe_2$, wherein we performed nudged elastic band (NEB) [31] calculations on the basis of the LCPAO (Linear Combination of Pseudo Atomic Orbitals) approach, as implemented in the OPENMX code [32]. A Perdew-Burke-Ernzerhof exchange-correlation functional [33] has been applied. The Projected Augmented Wave method from the VASP code [34,35] was used, taking into account both spin-orbit coupling and scalar-relativistic corrections. The lithium ground-state energies were estimated by approximating the NEB diffusion energy barriers with an anisotropic harmonic oscillator potential. The crystal structures were visualized using VESTA [36].

We find the stable $^8Li^+$ site to be at the 2a Wyckoff position [Fig. 1(b)]. This site has a D_{3d} point group symmetry, so a nonzero EFG is expected, which would result in a splitting of the ^{8}Li quadrupolar transitions. Possible charge states of the implanted lithium, namely, $^8Li^+$ and neutral $^8Li^0$, are accounted for by considering charged and neutral supercells, respectively [13,37,38]. We find the same 2a stopping site and the absence of induced spin polarization at the ^{8}Li site [Fig. 1(d)] for both charged states. The resulting calculated diffusion energy barriers along the paths indicated in Fig. 1(b) are shown in Fig. 1(c). We note that in MoS_2 the diffusion of Li between 2a sites was found to occur via a tetrahedral site above a Mo atom [39,40] and a similar stable Li site has also been considered in $2H$-$MoTe_2$ [41]. However, in our calculations, a diffusion path via the 6g site in between two Te atoms is found to be preferable.

IV. RESULTS

Typical ^{8}Li β-NMR line shapes measured in a 6.55 T out-of-plane field at different temperatures are shown in Fig. 2(a). They consist of a broad central resonance at all temperatures with small quadrupolar satellites appearing below 260 K. Above this temperature, the quadrupolar splitting cannot be resolved. In order to accurately determine the satellite frequencies, we performed frequency-comb measurements, representative spectra of which are shown in Fig. 2(b). Except near room temperature, the peaks at $\nu = \nu_q$ and $\nu = 3\nu_q$ are always clearly visible, whereas the peak at $\nu = \nu_q/3$ is only visible in the vicinity of 260 K. We have extracted the value of ν_q by fitting the frequency-comb spectra to a sum of two or three Lorentzian peaks, depending on whether the signal at $\nu = \nu_q/3$ was clearly resolved or not. The baseline from the central peak was phenomenologically parametrized by a second-order polynomial, which gives a good agreement with the observed spectra, as shown by the solid lines in Fig. 2(b). We then analyzed the resonance line shapes [Fig. 2(a)] by fitting them to a sum of five Lorentzian peaks: a central one and four corresponding to the quadrupolar splitting. The position and width of the latter were assumed to be given by the values extracted from the fits to the comb spectra. At the two highest temperature points, where no clear quadrupolar splitting is visible in the line shape or frequency comb, a single Lorentzian was assumed.

The resulting temperature dependence of the resonance line parameters is shown in Fig. 3. The temperature dependence of the quadrupolar splitting in Fig. 3(a) exhibits a power-law behavior $\nu_q = \nu_{q0}(1 - cT^{3/2})$, where $\nu_{q0} = 3.603(4)$ kHz and $c = 2.33(7) \times 10^{-5}$ kHz/$K^{3/2}$ were determined via weighted least-squares minimization. The resulting curve is shown as a dashed line in Fig. 3(a). Phenomenologically, this is the typical temperature dependence of the quadrupolar frequency in the presence of thermally activated phonons [42,43]. The quadrupolar contribution to the spectral weight was estimated by the sum of amplitudes of the four

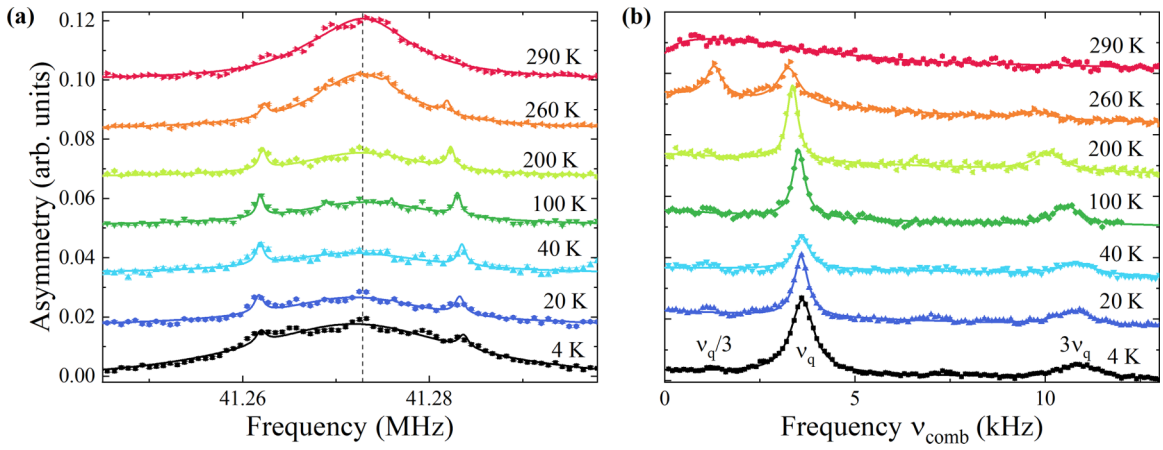

FIG. 2. (a) Representative ^{8}Li β-NMR line shapes in $2H$-$MoTe_2$ measured in an out-of-plane magnetic field of 6.55 T at various temperatures. The spectra are vertically offset for clarity. The broad central peak arises from dynamically averaged environments, while the smaller satellites correspond to quadrupolar splitting due to the local electric field gradient at the ^{8}Li site. The solid lines are fits as described in the text, and the vertical dashed line indicates the reference frequency from MgO. (b) Frequency-comb ^{8}Li β-NMR spectra measured in the same field as a function of the comb frequency ν_{comb}. This technique simultaneously excites multiple quadrupolar transitions, enhancing sensitivity to the quadrupolar-split components. Peaks at $\nu_{comb} = \nu_q/3$, ν_q, and $3\nu_q$ correspond to first-order quadrupolar transitions, enabling accurate determination of the quadrupolar frequency ν_q even when the satellites are weak or partially overlapped by the central line.

quadrupolar peaks relative to the sum of all five peaks and is shown in Fig. 3(b). Note that the central peak frequency ν_c shows only little temperature dependence [Fig. 3(c)], with its full width at half maximum, Δ_c, increasing with decreasing temperature [Fig. 3(d)].

Typical ^{8}Li SLR curves as a function of time in the presence of a 10 mT in-plane field are shown in Fig. 4(a). The relaxation of the $^8Li^+$ ensemble occurs on a timescale of seconds, with distinct fast- and slow-relaxing contributions. From the raw data, the relaxation seems to be slowest for the curve at 50 K. The time dependence of the SLR curves in Fig. 4(a) can be described by a sum of two exponential depolarization functions, representing a fast ($1/T_{1,f}$)- and a slow ($1/T_{1,s}$)-relaxing component:

$$A(t) = A_0(f_{slow}e^{-t/T_{1,s}} + (1 - f_{slow})e^{-t/T_{1,f}}), \qquad (1)$$

where f_{slow} is the contribution of the slow-relaxing fraction. The initial asymmetry A_0 was assumed to be temperature independent. Equation (1) was then convoluted with the duration of the beam pulse [18]. Such a biexponential behavior is the simplest model that can adequately describe the data [44], while avoiding overparametrization of the fits.

The relaxation rates obtained from the fits are shown in Figs. 4(c) and 4(d) and exhibit two peaks: One around 240 K and the second at ∼15 K, the latter coinciding with a local minimum in f_{slow} [Fig. 4(b)]. Note that any fluctuations coupling to the ^{8}Li spin and passing through the Larmor frequency (∼63 kHz at 10 mT) as a function of temperature could produce such peaks. An Arrhenius law was used to fit the low-temperature flank of the 240 K SLR peak, giving an activation energy $E_A \sim 0.2$ eV, as shown in Fig. 4(c). This increase in SLR with the observed energy scale could be attributed to the onset of ^{8}Li diffusion, as previously reported in other vdW materials [45]. Such a mechanism would result in dynamic changes of the EFG experienced by ^{8}Li, coupling to its quadrupolar moments and thereby enhancing its SLR. However, in this case, it is inconsistent with the absence of motional narrowing in the corresponding line shapes [Fig. 2(a)]. In addition, the extracted activation energy of 0.2 eV is much smaller than the estimated hopping barrier of ≈1 eV predicted from DFT [Fig. 1(c)]. A possible explanation for this temperature dependence is discussed below.

V. DISCUSSION

Although the two components in the line shape could suggest that there are two inequivalent Li states present in the sample, there are several indications that this is not due to two different crystallographic ^{8}Li stopping sites. From a theoretical perspective, the calculations identify only one candidate site, and there are no Wyckoff positions with a cubic point group symmetry in space group 194 that could explain the absence of an EFG on the broad central peak. Experimentally, the broad central line has a similar width to the total quadrupole splitting $3\nu_q$, which points to a scenario where an additional broadening affects the quadrupolar splitting. But, more importantly, the quadrupolar fraction in Fig. 3(b) seems to be strongly correlated with the slow fraction of the SLR [Fig. 4(b)], which indicates that the absence of a detectable quadrupolar splitting is related to the presence of fast dynamics. The exact microscopic mechanism of the two ^{8}Li states is currently unknown. Possibilities include diffusional dynamics in a local cage or multiple charge states of the implanted lithium. In addition to the expected $^8Li^+$ state, a neutral $^8Li^0$ state could form by capturing an electron from the host [46]. The charged $^8Li^+$ ion is expected to exhibit a well-defined quadrupolar interaction due to the local electric field gradient, whereas neutral $^8Li^0$, which carries an additional electron, may experience strong hyperfine-mediated fluctuations and enhanced electronic screening. This can lead to faster spin-lattice relaxation and a reduced or unresolved quadrupolar splitting, consistent with the observed correlation between the

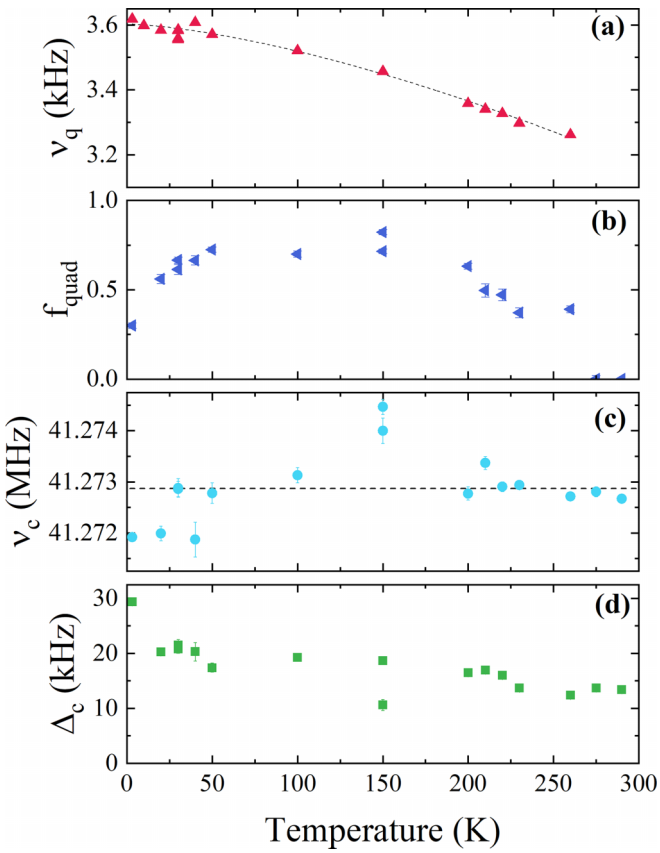

FIG. 3. Temperature dependence of resonance parameters extracted from fits to the β-NMR spectra: (a) quadrupolar frequency ν_q, (b) relative spectral weight of the quadrupolar satellites (f_{quad}), (c) central resonance frequency ν_c, and (d) full width at half maximum Δ_c of the central peak. The dashed line in panel (a) shows a $T^{3/2}$ dependence, characteristic of phonon-driven changes in the electric field gradient. The dashed line in panel (c) indicates the MgO reference frequency. The decrease of f_{quad} and the broadening of the central peak at higher temperatures are consistent with increasing dynamical fluctuations of the ^{8}Li environment.

fast-relaxing fraction and the diminished quadrupolar signal. Long-range ^{8}Li diffusion is highly unlikely since we observe no motional narrowing at high temperature while the activation energy is much lower than that calculated for hopping between two neighboring ^{8}Li sites. If the bound electron in the neutral state corresponds to a very shallow donor state, then the associated large electronic orbital might explain the absence of a pronounced hyperfine shift. Note that both a small hyperfine coupling and a relatively small quadrupolar splitting are typical for ^{8}Li$^+$ in the vdW gap of nonmagnetic layered compounds [45,47–49].

In light of the magnetic state observed by μSR [10,13], it is important to consider whether there are similar magnetic signatures detectable with β-NMR. However, the behavior of the ^{8}Li SLR at low temperature is inconsistent with a strong local static magnetic field being present at the ^{8}Li position. Such a local field would depolarize the ^{8}Li spin completely on a timescale of milliseconds. The size of the local magnetic field in μSR at low temperature is ∼200 mT [10] and is associated with a magnetic muonium state at the 2a Wyckoff position [13], which is the same as the ^{8}Li$^+$ stopping site. Given the smaller gyromagnetic ratio of ^{8}Li ($\gamma_{^8\mathrm{Li}}/2\pi = 6.3016\,\mathrm{MHz}/T$, with $\gamma_{^8\mathrm{Li}}/\gamma_\mu \sim 4.7\,\%$), a similar local field would still cause a precession with $\gtrsim$1.2 MHz. This is too fast to be detected given the limited time resolution of ^{8}Li β-NMR. Moreover, the decoherence or any broadening of such oscillations would rapidly depolarize the ^{8}Li. Both of these effects would manifest as an immediate loss of polarization at early times (cf. Ref. [50]). However, we do not observe such an instant depolarization of the ^{8}Li spin. Note that this argument can exclude both a ferromagnetic state and the presence of an ^{8}Li-induced electronic spin polarization, similar to that observed with muons [13]. An antiferromagnetic state with a vanishing or compensated net local field at the ^{8}Li site may also be considered. However, at the phase transition, one would expect critical fluctuations to be present, which should cross the ^{8}Li Larmor frequency and lead to a SLR peak at T_{N} (cf. 1T-CrSe$_2$ [51]), which would not be suppressed by the low applied field in our measurements. While the SLR peak around ∼15 K could be caused by magnetic fluctuations, it occurs at a temperature too low to be compatible with the magneticlike transition observed with μSR. Together with the absence of any magnetic signal in ^{125}Te-NMR [13], this serves as clear evidence that 2H-MoTe$_2$ does not exhibit intrinsic magnetic order.

The present results provide a consistent framework that reconciles earlier local-probe measurements on 2H-MoTe$_2$. While μSR detects magnetism associated with a neutral hydrogenlike muonium state that locally induces spin polarization in the host [10,13], our β-NMR measurements with positively charged ^{8}Li$^+$, which occupies a similar crystallographic site in the vdW gap, show no evidence of either intrinsic or impurity-induced magnetism. Together with the absence of magnetic signatures in ^{125}Te-NMR [13], this demonstrates that magnetism in 2H-MoTe$_2$ is not intrinsic but highly sensitive to the nature and charge state of the impurity. Since the crystals used here originate from the same batch as in Ref. [13], differences in sample quality or composition can be ruled out, and the contrasting behavior can be attributed to the fundamentally different electronic character of muonium and ^{8}Li$^+$ impurities.

VI. CONCLUSION

We have investigated isolated ^{8}Li impurities implanted into 2H-MoTe$_2$ using β-NMR and complementary DFT calculations. The ^{8}Li occupies the 2a Wyckoff position in the van der Waals gap but does not induce detectable magnetic polarization, in contrast to hydrogenlike muonium. Instead, we observe thermally activated local dynamics above ∼200 K, reflected in both the spin-lattice relaxation and the evolution of the resonance line shape. These dynamics may be caused by stochastic motion in a local cage. The frequency-comb method proves particularly effective for resolving the quadrupolar splitting even in the presence of a complex, multicomponent line shape.

Together, these results clarify that magnetism in 2H-MoTe$_2$ is not intrinsic but is strongly dependent on the electronic character and charge state of the impurity. This highlights the importance of impurity-specific electronic

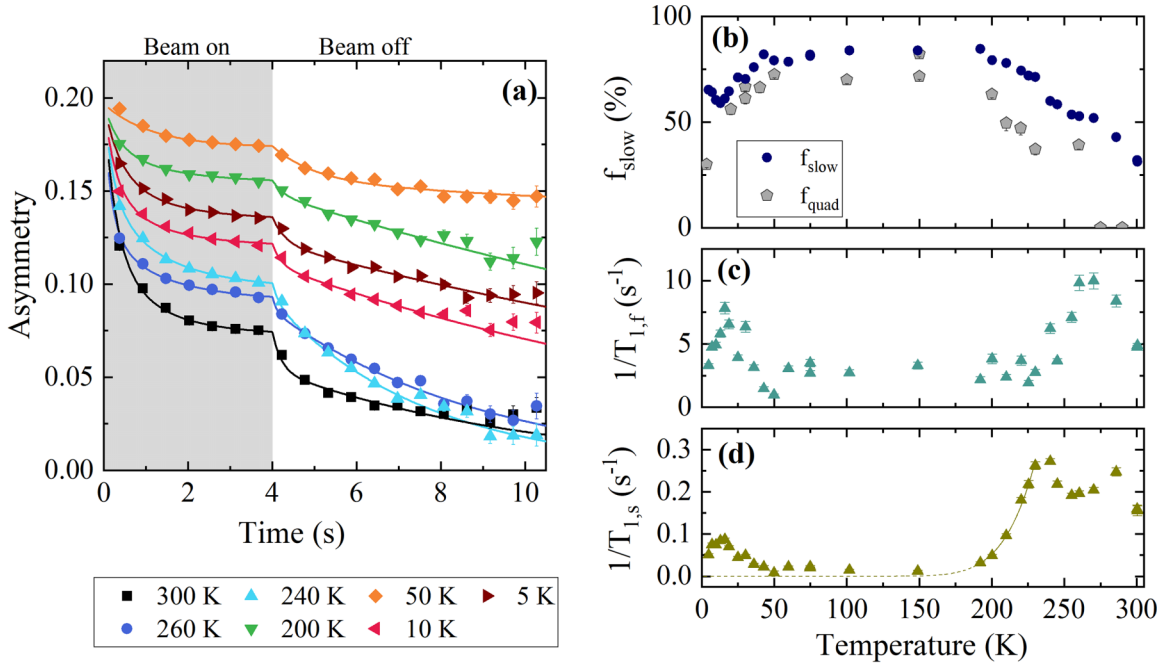

FIG. 4. (a) Representative spin-lattice relaxation data for ^{8}Li in 2H-MoTe$_2$ measured in an in-plane magnetic field of 10 mT. The shaded region indicates the 4 s beam-on period, after which the beam is turned off and relaxation is monitored. The solid lines are fits using a biexponential relaxation model. The temperature dependence of (b) the slowly relaxing fraction $f_{\rm slow}$, (c) the fast relaxation rate $1/T_{1,\rm f}$, and (d) the slow relaxation rate $1/T_{1,\rm s}$. The solid line in panel (d) is an Arrhenius fit to the low-temperature side of the peak near 240 K, yielding an activation energy of approximately 0.2 eV. For comparison, panel (b) also shows the relative quadrupolar spectral weight $f_{\rm quad}$ [from Fig. 3(b)], illustrating the correlation between the loss of resolved quadrupolar splitting and the onset of fast dynamical fluctuations.

structure in governing magnetic responses in layered semiconductors.

ACKNOWLEDGMENTS

The β-NMR experiments were performed at the TRIUMF Centre for Materials and Molecular Science. We thank G. D. Morris, C. D. P. Levy, R. Li, B. Hitti, S. Daviel, and R. Abasalti for helpful discussions and technical support. J.A.K. and S.H. acknowledge support by the Swiss National Science Foundation (J.A.K.: SNF Grants No. 200021_165910 and No. P500PT_203159; S.H.: Grant No. 200021-159736). E.V.C. acknowledges funding by Saint Petersburg State University project for scientific investigations (Grant No. 125022702939-2). The work at Warwick was supported by EPSRC, UK, through Grant No. EP/M028771/1. D.F., V.L.K., and J.O.T. acknowledge support from a QuEST fellowship. A.C. and R.M.L.M. acknowledge the support of IsoSiM scholarships. Finally, we note that a preliminary version of some of these results was published as part of a Ph.D. thesis [52].

DATA AVAILABILITY

The data that support the findings of this study are available from the corresponding author upon reasonable request.

[1] S. Manzeli, D. Ovchinnikov, D. Pasquier, O. V. Yazyev, and A. Kis, 2D transition metal dichalcogenides, Nat. Rev. Mater. **2**, 17033 (2017).

[2] A. K. Geim and I. V. Grigorieva, Van der Waals heterostructures, Nature (London) **499**, 419 (2013).

[3] C. R. Rajamathi, U. Gupta, N. Kumar, H. Yang, Y. Sun, V. Süß, C. Shekhar, M. Schmidt, H. Blumtritt, P. Werner, B. Yan, S. Parkin, C. Felser, and C. N. R. Rao, Weyl semimetals as hydrogen evolution catalysts, Adv. Mater. **29**, 1606202 (2017).

[4] A. J. Grant, T. M. Griffiths, G. D. Pitt, and A. D. Yoffe, The electrical properties and the magnitude of the indirect gap in the semiconducting transition metal dichalcogenide layer crystals, J. Phys. C: Solid State Phys. **8**, L17 (1975).

[5] A. Conan, D. Delaunay, A. Bonnet, A. G. Moustafa, and M. Spiesser, Temperature dependence of the electrical conductivity and thermoelectric power in MoTe$_2$ single crystals, Phys. Status Solidi B **94**, 279 (1979).

[6] I. G. Lezama, A. Ubaldini, M. Longobardi, E. Giannini, C. Renner, A. B. Kuzmenko, and A. F. Morpurgo, Surface transport and band gap structure of exfoliated 2H-MoTe$_2$ crystals, 2D Mater. **1**, 021002 (2014).

[7] H. Xu, S. Fathipour, E. W. Kinder, A. C. Seabaugh, and S. K. Fullerton-Shirey, Reconfigurable ion gating of 2H-MoTe$_2$ field-effect transistors using poly(ethylene oxide)-CsClO$_4$ solid polymer electrolyte, ACS Nano **9**, 4900 (2015).

[8] Y. Ding, N. Zhou, L. Gan, X. Yan, R. Wu, I. H. Abidi, A. Waleed, J. Pan, X. Ou, Q. Zhang, M. Zhuang, P. Wang, X. Pan,

Z. Fan, T. Zhai, and Z. Luo, Stacking-mode confined growth of 2*H*-$MoTe_2/MoS_2$ bilayer heterostructures for UV-vis-IR photodetectors, Nano Energy **49**, 200 (2018).

[9] G. Li, Y. Xu, Z. Song, Q. Yang, Y. Zhang, J. Liu, U. Gupta, V. Süß, Y. Sun, P. Sessi, S. S. P. Parkin, B. A. Bernevig, and C. Felser, Obstructed surface states as the descriptor for predicting catalytic active sites in inorganic crystalline materials, Adv. Mater. **34**, 2201328 (2022).

[10] Z. Guguchia, A. Kerelsky, D. Edelberg, S. Banerjee, F. von Rohr, D. Scullion, M. Augustin, M. Scully, D. A. Rhodes, Z. Shermadini, *et al.*, Magnetism in semiconducting molybdenum dichalcogenides, Sci. Adv. **4**, eaat3672 (2018).

[11] Y. Ma, Y. Dai, M. Guo, C. Niu, J. Lu, and B. Huang, Electronic and magnetic properties of perfect, vacancy-doped, and nonmetal adsorbed $MoSe_2$, $MoTe_2$ and WS_2 monolayers, Phys. Chem. Chem. Phys. **13**, 15546 (2011).

[12] H. González-Herrero, J. M. Gómez-Rodríguez, P. Mallet, M. Moaied, J. J. Palacios, C. Salgado, M. M. Ugeda, J.-Y. Veuillen, F. Yndurain, and I. Brihuega, Atomic-scale control of graphene magnetism by using hydrogen atoms, Science **352**, 437 (2016).

[13] J. A. Krieger, D. Tay, I. P. Rusinov, S. Barua, P. K. Biswas, L. Korosec, T. Prokscha, T. Schmitt, N. B. M. Schröter, T. Shang, T. Shiroka, A. Suter, G. Balakrishnan, E. V. Chulkov, V. N. Strocov, and Z. Salman, Hydrogen-impurity-induced unconventional magnetism in semiconducting molybdenum ditelluride, Phys. Rev. Mater. **7**, 044414 (2023).

[14] Z. Lin, B. R. Carvalho, E. Kahn, R. Lv, R. Rao, H. Terrones, M. A. Pimenta, and M. Terrones, Defect engineering of two-dimensional transition metal dichalcogenides, 2D Mater. **3**, 022002 (2016).

[15] H. Li, C. Tsai, A. L. Koh, L. Cai, A. W. Contryman, A. H. Fragapane, J. Zhao, H. S. Han, H. C. Manoharan, F. Abild-Pedersen, J. K. Nørskov, and X. Zheng, Activating and optimizing MoS_2 basal planes for hydrogen evolution through the formation of strained sulphur vacancies, Nat. Mater. **15**, 48 (2016).

[16] S. McDonnell and P. Reinke, Defects in transition metal dichalcogenides, in *Defects in Two-Dimensional Materials, Materials Today*, edited by R. Addou and L. Colombo (Elsevier, Amsterdam, Netherlands, 2022), Chap. 4, pp. 89–117.

[17] Z. Guguchia, F. von Rohr, Z. Shermadini, A. T. Lee, S. Banerjee, A. R. Wieteska, C. A. Marianetti, B. A. Frandsen, H. Luetkens, Z. Gong, *et al.*, Signatures of the topological s^{+-} superconducting order parameter in the type-II Weyl semimetal T_d-$MoTe_2$, Nat. Commun. **8**, 1082 (2017).

[18] Z. Salman, R. F. Kiefl, K. H. Chow, M. D. Hossain, T. A. Keeler, S. R. Kreitzman, C. D. P. Levy, R. I. Miller, T. J. Parolin, M. R. Pearson, H. Saadaoui, J. D. Schultz, M. Smadella, D. Wang, and W. A. MacFarlane, Near-surface structural phase transition of $SrTiO_3$ studied with zero-field β-detected nuclear spin relaxation and resonance, Phys. Rev. Lett. **96**, 147601 (2006).

[19] G. D. Morris, W. A. MacFarlane, K. H. Chow, Z. Salman, D. J. Arseneau, S. Daviel, A. Hatakeyama, S. R. Kreitzman, C. D. P. Levy, R. Poutissou, R. H. Heffner, J. E. Elenewski, L. H. Greene, and R. F. Kiefl, Depth-controlled β-NMR of ^{8}Li in a thin silver film, Phys. Rev. Lett. **93**, 157601 (2004).

[20] G. D. Morris, β-NMR, Hyperfine Interact. **225**, 173 (2014).

[21] C. D. P. Levy, M. R. Pearson, R. F. Kiefl, E. Mané, G. D. Morris, and A. Voss, Laser polarization facility, Hyperfine Interact. **225**, 165 (2014).

[22] W. A. MacFarlane, Implanted-ion βNMR: A new probe for nanoscience, Solid State Nucl. Magn. Reson. **68–69**, 1 (2015).

[23] W. A. MacFarlane, Status and progress of ion-implanted βNMR at TRIUMF, Z. Phys. Chem. **236**, 757 (2022).

[24] A. Hatakeyama, Y. Hirayama, J. A. Behr, H. Izumi, C. D. P. Levy, D. Melconian, and T. Shimoda, Optical pumping at the ISAC polarizer, in *Polarized Sources and Targets*, edited by V. P. Derenchuk and B. von Przewoski (World Scientific, Singapore, 2002), pp. 339–343.

[25] W. Eckstein, in *Computer Simulation of Ion-Solid Interactions*, edited by U. Gonser, A. Mooradian, R. M. Osgood, M. B. Panish, H. Sakaki, and H. K. V. Lotsch, Springer Series in Materials Science (Springer-Verlag, Berlin, 1991).

[26] T. Minamisono, T. Ohtsubo, S. Fukuda, I. Minami, Y. Nakayama, M. Fukuda, K. Matsuta, and Y. Nojiri, New nuclear quadrupole resonance technique in β-NMR, Hyperfine Interact. **80**, 1315 (1993).

[27] J. R. Adelman, D. Fujimoto, M. H. Dehn, S. R. Dunsiger, V. L. Karner, C. D. P. Levy, R. Li, I. McKenzie, R. M. L. McFadden, G. D. Morris, M. R. Pearson, M. Stachura, E. Thoeng, J. O. Ticknor, N. Ohashi, K. M. Kojima, and W. A. MacFarlane, Nuclear magnetic resonance of ^{8}Li ions implanted in ZnO, Phys. Rev. B **106**, 035205 (2022).

[28] H. J. Stöckmann, H. Ackermann, D. Dubbers, M. Grupp, and P. Heitjans, Elektrische quadrupolwechselwirkungen von ^{20}F im MgF_2-einkristall, Z. Phys. **269**, 47 (1974).

[29] H. Ackermann, D. Dubbers, M. Grupp, P. Heitjans, G. Z. Putlitz, and H. J. Stöckmann, Static electric quadrupole interaction of the β-emitter ^{20}F produced by capture of polarized neutrons in MgF_2 single crystals, Phys. Lett. B **41**, 143 (1972).

[30] A. Suter and B. M. Wojek, Musrfit: A free platform-independent framework for μSR data analysis, Phys. Proc. **30**, 69 (2012).

[31] G. Henkelman and H. Jónsson, Improved tangent estimate in the nudged elastic band method for finding minimum energy paths and saddle points, J. Chem. Phys. **113**, 9978 (2000).

[32] T. Ozaki, Variationally optimized atomic orbitals for large-scale electronic structures, Phys. Rev. B **67**, 155108 (2003).

[33] J. P. Perdew, K. Burke, and M. Ernzerhof, Generalized gradient approximation made simple, Phys. Rev. Lett. **77**, 3865 (1996).

[34] G. Kresse and J. Furthmüller, Efficient iterative schemes for *ab initio* total-energy calculations using a plane-wave basis set, Phys. Rev. B **54**, 11169 (1996).

[35] G. Kresse and D. Joubert, From ultrasoft pseudopotentials to the projector augmented-wave method, Phys. Rev. B **59**, 1758 (1999).

[36] K. Momma and F. Izumi, *VESTA 3* for three-dimensional visualization of crystal, volumetric and morphology data, J. Appl. Cryst. **44**, 1272 (2011).

[37] J. S. Möller, D. Ceresoli, T. Lancaster, N. Marzari, and S. J. Blundell, Quantum states of muons in fluorides, Phys. Rev. B **87**, 121108(R) (2013).

[38] F. Bernardini, P. Bonfà, S. Massidda, and R. De Renzi, *Ab initio* strategy for muon site assignment in wide band gap fluorides, Phys. Rev. B **87**, 115148 (2013).

[39] J. Shuai, H. D. Yoo, Y. Liang, Y. Li, Y. Yao, and L. C. Grabow, Density functional theory study of Li, Na, and Mg intercalation and diffusion in MoS_2 with controlled interlayer spacing, Mater. Res. Express **3**, 064001 (2016).

[40] A. N. Enyashin and G. Seifert, Density-functional study of Li_xMoS_2 intercalates ($0 \leqslant x \leqslant 1$), Comput. Theor. Chem. **999**, 13 (2012).

[41] M. R. Panda, R. Gangwar, D. Muthuraj, S. Sau, D. Pandey, A. Banerjee, A. Chakrabarti, A. Sagdeo, M. Weyland, M. Majumder, Q. Bao, and S. Mitra, High performance lithium-ion batteries using layered $2H$-$MoTe_2$ as anode, Small **16**, 2002669 (2020).

[42] J. Christiansen, P. Heubes, R. Keitel, W. Klinger, W. Loeffler, W. Sandner, and W. Witthuhn, Temperature dependence of the electric field gradient in noncubic metals, Z. Phys. B **24**, 177 (1976).

[43] A. V. Nikolaev, N. M. Chtchelkatchev, D. A. Salamatin, and A. V. Tsvyashchenko, Towards an *ab initio* theory for the temperature dependence of electric field gradients in solids: Application to hexagonal lattices of Zn and Cd, Phys. Rev. B **101**, 064310 (2020).

[44] For example, a stretched exponential $A(t) = A_0 e^{-(t/T_1)^\beta}$ fails, because the stretching coefficient β converges to nonphysical values of $\beta \sim 0.2$.

[45] R. M. L. McFadden, A. Chatzichristos, K. H. Chow, D. L. Cortie, M. H. Dehn, D. Fujimoto, M. D. Hossain, H. Ji, V. L. Karner, R. F. Kiefl, C. D. P. Levy, R. Li, I. McKenzie, G. D. Morris, O. Ofer, M. R. Pearson, M. Stachura, R. J. Cava, and W. A. MacFarlane, Ionic and electronic properties of the topological insulator Bi_2Te_2Se investigated via β-detected nuclear magnetic relaxation and resonance of ^{8}Li, Phys. Rev. B **99**, 125201 (2019).

[46] W. A. MacFarlane, R. M. L. McFadden, S. L. Spencer, A. Chatzichristos, J. O. Ticknor, D. L. Cortie, M. H. Dehn, S. R. Dunsiger, D. Fujimoto, Z. H. Jang, V. L. Karner, R. F. Kiefl, G. D. Morris, and M. Stachura, Lithium ion dynamics in synthetic quartz studied via the NMR of implanted $^8Li^+$, Phys. Rev. B **112**, 014103 (2025).

[47] D. Wang, M. D. Hossain, Z. Salman, D. Arseneau, K. H. Chow, S. Daviel, T. A. Keeler, R. F. Kiefl, S. R. Kreitzman, C. D. P. Levy, G. D. Morris, R. I. Miller, W. A. MacFarlane, T. J. Parolin, and H. Saadaoui, β-detected NMR of ^{8}Li in the normal state of $2H$-$NbSe_2$, Phys. B **374**, 239 (2006).

[48] R. M. L. McFadden, A. Chatzichristos, D. L. Cortie, D. Fujimoto, Y. S. Hor, H. Ji, V. L. Karner, R. F. Kiefl, C. D. P. Levy, R. Li, I. McKenzie, G. D. Morris, M. R. Pearson, M. Stachura, R. J. Cava, and W. A. MacFarlane, Local electronic and magnetic properties of the doped topological insulators Bi_2Se_3:Ca and Bi_2Te_3:Mn investigated using ion-implanted ^{8}Li β-NMR, Phys. Rev. B **102**, 235206 (2020).

[49] J. Ticknor, Ion-implanted ^{8}Li nuclear magnetic resonance study of van der Waals layered materials, Ph.D. thesis, University of British Columbia, Vancouver, Canada, 2025, https://doi.org/10.14288/1.0447683.

[50] D. L. Cortie, T. Buck, M. H. Dehn, V. L. Karner, R. F. Kiefl, C. D. P. Levy, R. M. L. McFadden, G. D. Morris, I. McKenzie, M. R. Pearson, X. L. Wang, and W. A. MacFarlane, β-NMR investigation of the depth-dependent magnetic properties of an antiferromagnetic surface, Phys. Rev. Lett. **116**, 106103 (2016).

[51] J. O. Ticknor, I. Umegaki, R. M. L. McFadden, A. Chatzichristos, D. Fujimoto, V. L. Karner, R. F. Kiefl, S. Kobayashi, C. D. P. Levy, R. Li, G. D. Morris, M. R. Pearson, K. Yoshimura, J. Sugiyama, and W. A. MacFarlane, Investigation of ionic and anomalous magnetic behavior in $CrSe_2$ using ^{8}Li β-NMR, RSC Adv. **10**, 8190 (2020).

[52] J. A. Krieger, Doping and interface effects in topological materials, Ph.D. thesis, ETH Zurich, 2020, https://doi.org/10.3929/ethz-b-000460760.